Degradation by Hydrogen Peroxide of Metal-Nitrogen-Carbon Catalysts for Oxygen Reduction

Vincent Goellner, Vanessa Armel, Andrea Zitolo, Emiliano Fonda, Frédéric Jaouen

▶ **To cite this version:**

Vincent Goellner, Vanessa Armel, Andrea Zitolo, Emiliano Fonda, Frédéric Jaouen. Degradation by Hydrogen Peroxide of Metal-Nitrogen-Carbon Catalysts for Oxygen Reduction. Journal of The Electrochemical Society, 2015, 162 (6), pp.H403-H404. 10.1149/2.1091506jes . hal-01174287

HAL Id: hal-01174287
https://hal.science/hal-01174287

Submitted on 8 Jul 2015

HAL is a multi-disciplinary open access archive for the deposit and dissemination of scientific research documents, whether they are published or not. The documents may come from teaching and research institutions in France or abroad, or from public or private research centers.

L'archive ouverte pluridisciplinaire **HAL**, est destinée au dépôt et à la diffusion de documents scientifiques de niveau recherche, publiés ou non, émanant des établissements d'enseignement et de recherche français ou étrangers, des laboratoires publics ou privés.

PROOF COPY [JES-15-0443] 1091506JES

Degradation by Hydrogen Peroxide of Metal-Nitrogen-Carbon Catalysts for Oxygen Reduction

Vincent Goellner,[a,*] Vanessa Armel,[a,*] Andrea Zitolo,[b] Emiliano Fonda,[b] and Frédéric Jaouen[a,,z]**

[a]*Institut Charles Gerhardt Montpellier, UMR CNRS 5253, Agrégats, Interfaces et Matériaux pour l'Energie, Université Montpellier, 34095 Montpellier cedex 5, France*
[b]*Synchrotron SOLEIL, L'Orme des Merisiers Saint-Aubin - BP 48, 91192 Gif-sur-Yvette, France*

Fe-N-C and Co-N-C materials are promising catalysts for reducing oxygen in fuel cells. The degradation of such catalysts induced by H_2O_2 was investigated by contacting them ex situ with various amounts of H_2O_2. The degradation increased with increasing amounts of H_2O_2. The effect was most severe for Cr-N-C followed by Fe-N-C and last by Co-N-C. Treatment with H_2O_2 leads to diminished oxygen reduction activity at high potential and/or reduced transport properties at high current density in fuel cell. From spectroscopic characterisation, it was found that 66 and 80% of the CoN_xC_y and FeN_xC_y moieties present in pristine catalysts survived the extensive H_2O_2 treatment, respectively. In parallel, the activity for oxygen reduction was divided by ca 6–10 for Fe-N-C and by ca 3 for Co-N-C. The results suggest that the main degradation mechanism in fuel cell for such catalysts is due to a chemical reaction with H_2O_2 that is generated during operation. The super-proportional decrease of the oxygen reduction activity with loss of FeN_xC_y and CoN_xC_y moieties suggests either that only a small fraction of such moieties are initially located on the top surface, or that their turnover frequency for oxygen reduction was drastically reduced due to surface oxidation by H_2O_2.
© The Author(s) 2015. Published by ECS. This is an open access article distributed under the terms of the Creative Commons Attribution Non-Commercial No Derivatives 4.0 License (CC BY-NC-ND, http://creativecommons.org/licenses/by-nc-nd/4.0/), which permits non-commercial reuse, distribution, and reproduction in any medium, provided the original work is not changed in any way and is properly cited. For permission for commercial reuse, please email: oa@electrochem.org. [DOI: 10.1149/2.1091506jes] All rights reserved.

Manuscript submitted February 5, 2015; revised manuscript received March 11, 2015. Published 00 0, 2015. This was Paper 1589 presented at the San Francisco, California, Meeting of the Society, October 27–November 1, 2013.

Electrochemical energy conversion devices are expected to play an increasing role for stationary and transportation applications as well as for reversible energy storage. Among the various applications already in use or contemplated for electrochemical devices, the transportation sector is the most demanding in terms of energy density, power density and cost.1 Driving a full-size car over 100 km requires ca 13 kWh of mechanical energy.[2] While batteries are more efficient than fuel cells, the higher energy density of H_2/air fuel cells relative to the lithium-ion battery (1.8 kWh per kg of H_2-reservoir at 690 bars; compared to 0.2 kWh per kg of Li-ion battery pack) is critical for designing a system that can propel a car over 500 km without refuelling or recharging.[2-3] Hence, the polymer electrolyte membrane fuel cell (PEMFC) is today the most promising electrochemical device for replacing internal combustion engines, with uncompromised driving range and power density.[3] Mid-term remaining challenges for PEMFCs are increased durability and reduced cost, while a longer-term challenge is the replacement of the rare and expensive platinum element by catalysts based on Earth-abundant metals.[1,4-5] Today, ca 80–90% of the mass of Pt in a PEMFC stack is placed at the cathode due to the sluggish oxygen reduction reaction (ORR) compared to fast hydrogen oxidation at the anode. Based on projections for mass production, Pt-based catalysts in today's PEMFC technology are expected to account for ca 50% of the material's cost of a fuel cell stack.[4,6] Significantly reducing the Pt loading in cathodes or eliminating the platinum metal altogether from ORR catalysts are two possible approaches to tackle this cost problem.[3,5]

While the concept of ORR catalysis by materials or molecules comprising Fe or Co, nitrogen and carbon elements is known since 1964,[7] breakthroughs in the ORR activity and fuel cell performance that were necessary to seriously consider Fe(Co)-N-C catalysts as potential substitutes to platinum in the acidic environment of PEMFCs were reported only after 2008.[2,8–14] While major advances in the ORR activity and power density of PEMFC comprising Fe(Co)-N-C based cathodes have been reported, the next grand scientific challenges are i) improved understanding of the structure of the active sites and ii) improved understanding of the degradation mechanisms. Depending on the latter, mitigation approaches might be very different: i) system-based solutions to avoid the transient high-potential polarization during start-up and shutdown, ii) catalyst-based approaches in order to avoid the formation of H_2O_2 during ORR or to endow the catalysts with a higher graphitic character, iii) novel cathode designs in order to stabilize its electrical, hydrophilic and diffusion properties. A restricted number of studies have focused on the degradation mechanisms of Fe(Co)-N-C catalysts.[15–28] Fe-N-C catalysts pyrolyzed in NH_3 have shown the highest initial activity and power performance thus far, but degrade very quickly in PEMFC, mostly due to a protonation and anion-binding effect of highly-basic surface N-groups that are characteristic of NH_3 pyrolysis.[16] Fe(Co)-N-C catalysts synthesized at high temperature in inert gas are initially less active but are more stable in PEMFC.[8–10,15,26] Disentangling the various degradation phenomena of Fe(Co)-N-C cathodes occurring during PEMFC operation is complex. Water flooding, changes of the hydrophilic properties of the cathode, loss of a fraction of the active sites through dissolution or via oxidative attacks generated by either the cathode potential, H_2O_2 or radical oxygen species (ROS) formed between H_2O_2 and the transition-metal-based active sites may all account to some degree for the overall decline of the cathode performance with time. In a first attempt to disentangle these phenomena, we recently investigated on a well-defined Fe-N-C catalyst the degradation incurred by high-voltage cycling.[21] This phenomenon is the least complex one to separately investigate from other degradation routes since it is not linked to the ORR. It was concluded that the FeN_xC_y moieties initially present in the Fe-N-C catalyst were not immediately destroyed after a polarization up to 1.4–1.5 V vs. RHE. However, bulk oxidation of the carbon matrix in which these active sites are embedded ultimately lead to the massive dissolution of FeN_xC_y moieties. In addition, increased electric resistance of the cathode layer after high potential cycling also contributed to the decline of the cathode performance.[21] Due to the integration of $Fe(Co)N_xC_y$ moieties at the edge of graphene sheets or within the sheets, these materials are intrinsically more prone to degradation when subjected to high electric potential than Pt/C catalysts. More graphitic matrices may be resorted to for synthesizing Fe(Co)-N-C catalysts. However, it is notoriously difficult to achieve a high density of $Fe(Co)N_xC_y$ moieties in highly graphitic substrates via pyrolysis.[23,29] Mitigation of the degradation induced by high-voltage

*Electrochemical Society Student Member.
**Electrochemical Society Active Member.
zE-mail: frederic.jaouen@univ-montp2.fr

Author Proof

on Fe(Co)-N-C catalysts should therefore be most effective by focusing on the causes of the high-voltage transients, namely i) the purging of uncombusted H_2 at the anode with air and ii) the non-selectivity of platinum for hydrogen oxidation.[30–32]

The present work focuses on the oxidative attack of Me-N-C catalysts by minute amount of H_2O_2 that is produced due to the incomplete electro-reduction of O_2 to H_2O during fuel cell operation. This degradation mechanism can probably not be dealt with at a system level and is therefore an inescapable issue for Me-N-C catalysts. While the % H_2O_2 produced during ORR is often not much higher on Fe(Co)-N-C than on Pt/C catalysts,[25–27,33–34] the residence time of H_2O_2 in the electrode may be longer with Fe(Co)-N-C catalysts due to their extremely poor activity for the electro-reduction of H_2O_2 to H_2O,[33,35] and poor activity for the chemical disproportionation of H_2O_2.[27,33,35–36] Chemical disproportionation of H_2O_2 is ca two orders of magnitude faster at high pH for such catalysts,[36] highlighting the possibility to recycle H_2O_2 at high pH but impossibility to do so at low pH. In contrast, platinum is an excellent catalyst for both the four-electron reduction of O_2 to H_2O and the two-electron reduction of H_2O_2 to H_2O.[33,37] The important difference between the durability of Pt/C and Fe(Co)-N-C catalysts in PEMFC may thus stem from their different reactivity toward H_2O_2. Moreover, chemical disproportionation of H_2O_2 on Fe(Co)-N-C catalysts via Fenton chemistry might produce a significant amount of radical oxygen species (ROS).[38–40] While suspected, the role of H_2O_2 in the degradation of Fe(Co)-N-C based cathodes during steady-state operation of a PEMFC has not yet been investigated in depth. Early work by Wiesener showed that addition for every 100 h of a given aliquot of H_2O_2 to the electrolyte lead to a faster degradation of a Co-N-C catalyst.[41] Ex situ chemical degradation of Fe-N-C catalysts with H_2O_2 was investigated in 2003 by Lefèvre.[25] A series of catalysts were immersed in H_2O_2 solutions of various concentrations. The ORR activities measured with a rotating-disk electrode (RDE) were shown to have strongly decreased. More recently, Zelenay's group applied a different ex situ H_2O_2 treatment, keeping the H_2O_2 concentration fixed but varying the duration of immersion of the catalyst.[26] In addition to measuring the ORR activity in RDE before and after the treatments, also the elemental composition was determined by X-ray photoelectron spectroscopy (XPS). A comprehensive understanding of the degradation mechanism of Me-N-C catalysts upon contact with H_2O_2 solution is however still lacking, especially regarding spectroscopic changes of the transition metal coordination.

In the present work, we synthesized a Fe-N-C, a Co-N-C and a Cr-N-C catalyst and contacted them with various amounts of H_2O_2 corresponding to ratios of mol H_2O_2 per mass of catalyst ranging over ca two orders of magnitudes. The ORR activities of the catalysts before and after H_2O_2 treatment were determined with RDE and in PEMFC. The pristine and treated materials were characterized with X-ray diffraction, X-ray absorption spectroscopy, X-ray photoelectron spectroscopy and, for Fe-N-C, with ^{57}Fe Mössbauer spectroscopy.

Experimental

Synthesis.— Catalyst precursors were prepared via a dry ballmilling approach from a Zn(II) zeolitic imidazolate framework ($ZnN_4C_8H_{12}$, Basolite Z1200 from BASF, labelled ZIF-8), Fe(II) acetate (Fe(II)Ac), Co(II)Ac, Cr(II)Ac and 1,10-phenanthroline. The Fe-N-C and Co-N-C catalysts were synthesized identically: weighed amounts of the dry powders of Fe(II)Ac (or Co(II)Ac), phenanthroline and ZIF-8 were poured into a ZrO_2 crucible. Then, 100 zirconium-oxide balls of 5 mm diameter were added and the crucible was sealed under air and placed in a planetary ball-miller (FRITSCH Pulverisette 7 Premium) to undergo 4 cycles of 30 min of ballmilling at 400 rpm. The resulting catalyst precursor was pyrolyzed at 1050°C in Ar for 1 h. The catalyst precursors contained 1 wt% of metal and the mass ratio of phenanthroline to ZIF-8 was 20/80.[9,21] The mass loss during pyrolysis was 60–65 wt%, leading to Fe and Co contents of 2.5–2.9 wt%. The catalyst precursor for Cr-N-C was prepared identically, but the pyrolysis was performed under flowing NH_3 at 950°C for 15 min.

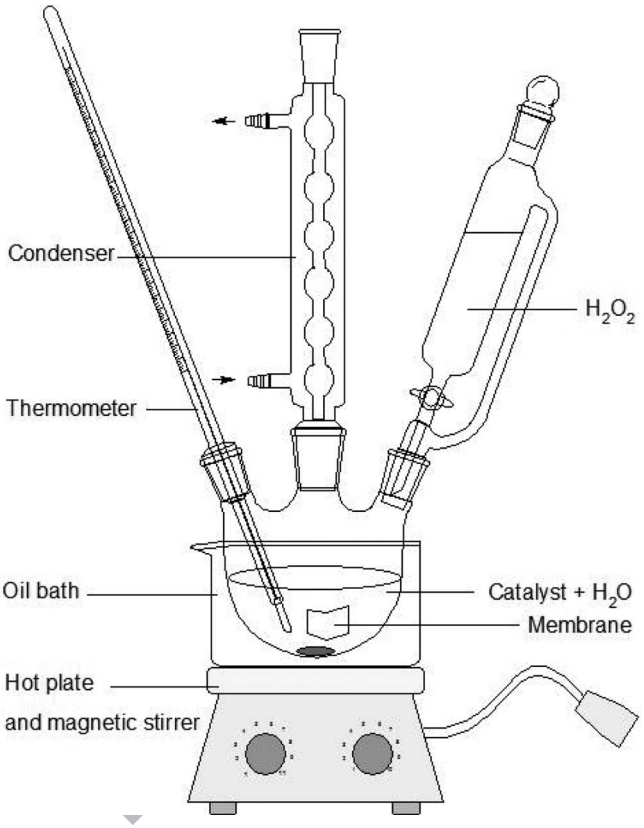

Figure 1. Scheme of the experimental setup used for ex situ H_2O_2 degradation.

When pyrolyzed in Ar, the initial ORR activity of Cr-N-C was too low to be of interest. The resulting Cr-based catalyst was then acid washed in a pH 1 sulphuric acid solution and copiously washed with de-ionized water. The acid washing was applied only to Cr-N-C in order to compare its ORR activity to the Ar-pyrolyzed Fe- and Co-N-C catalysts. It is known that pyrolysis in NH_3 leads to a higher initial ORR activity, mostly due to the presence of highly basic surface N-groups.[16] This promotion of ORR activity due to the high basicity of N-groups is usually suppressed after an acid wash, which protonates basic N-groups followed by anion adsorption. The mass loss during pyrolysis for the Cr-based catalyst precursor was 85–90 wt%, leading to 8–10 wt% Cr in Cr-N-C.

Chemical treatment with hydrogen peroxide.— 100 mg of catalyst was dispersed and stirred in (500 – X) ml of deionized water heated to 80°C under reflux. A piece of Nafion 117 membrane with area 4.84 cm^2 was also immersed in solution in order to serve as an indicator for ROS. The scalar X represent the total volume of 30 wt% H_2O_2 solution that was added to reach the desired number of mol H_2O_2 per mg of catalyst. This volume was systematically divided in four aliquots of X/4 ml, each aliquot being added with a one hour time interval. Once the total desired volume of H_2O_2 had been added, the solution was stirred for 24 h at 80°C under reflux and then allowed to cool down to room temperature. The entire experimental setup can be visualized in Fig. 1. For example, in order to reach a ratio of 10^{-2} mol H_2O_2 per mg of catalyst, four aliquots of 25 ml each of 30 wt% H_2O_2 solution were added every hour to a solution initially containing 100 mg of catalyst dispersed in 500-(4 × 25) ml of deionized water. In the present study, the ratio of mol H_2O_2 per mg catalyst was spanned from 5×10^{-4} to 2×10^{-2} by changing the cumulative volume of 30 wt% H_2O_2 from 5 to 200 ml. Each H_2O_2 treatment was terminated with a one hour sonication of the solution to solubilize fluoride ions originating from membrane degradation. The Nafion membrane piece

Author

was removed and the solution filtrated using a Büchner setup with a 220 nm pore-sized filter. The filtrate was stored for fluoride ion analysis while the collected catalyst powder was copiously washed with de-ionized water (ca one litre) before overnight drying at 90°C. The collected mass of dry catalyst powder was then weighed while the fluoride ion concentration in the filtrate was measured using an ion selective electrode. To avoid any interference of the pH, the electrolyte solution was adjusted with the appropriate ionic strength adjustment buffer (TISAB IV from Sigma-Aldrich) in order to keep the pH in the range of 5–7. TISAB solution also prevents complexation of fluoride ions with any iron or other trace metals present in solution.

Structural characterization.— Metal K-edge X-ray absorption spectra were recorded at room temperature at SAMBA beamline of Synchrotron SOLEIL. The beamline is equipped with a sagittaly focusing Si 220 monochromator and two Pd-coated collimating mirrors. The mirrors have been used to remove X-rays harmonics. The catalysts were pelletized as disks of 10 mm diameter using a 50/50 mass ratio of Teflon powder (1 μm particle size) and catalyst. The spectra were recorded in transmission mode and the energy was calibrated with the corresponding metal foils to correct any change in beam energy during the experiments. All experimental spectra were normalized and analyzed identically with Athena software in order to derive the XANES and Fourier-transform EXAFS spectra. X-ray diffraction was conducted using a PANanalytical X'Pert Pro powder X-ray diffractometer. XPS spectra were recorded with a Physical Electronics PHI 5701 spectrometer. Non-monochromatic Mg K_α X-ray was used as the excitation source. For the pristine and H_2O_2-treated Fe-N-C catalysts, ^{57}Fe Mössbauer spectra were measured with a source of ^{57}Co in rhodium. The measurements were performed keeping both the source and the absorber at room temperature. The spectrometer was operated with a triangular velocity waveform, and a NaI scintillation detector was used for detecting the γ-rays. Velocity calibration was performed with an α-Fe foil.

Electrochemical characterization.— Electrochemical activity of the catalysts toward the ORR was determined using the RDE technique. A catalyst ink including 10 mg of catalyst, 109 μl of a 5 wt% Nafion solution containing 15–20% water, 300 μl of ethanol and 36 μl of de-ionized water was sonicated and mixed using a vortex. An aliquot of 7 μl was deposited on the glassy-carbon disk (0.196 cm^2) resulting in a catalyst loading of 800 $\mu g \cdot cm^{-2}$. The working electrode with the deposited catalyst layer was used in a three-electrode cell setup connected to a potentiostat (Versastat 3, AMETEK) and rotator (MSR, Pine Instruments). The counter electrode and reference electrode were a graphite rod and a reversible hydrogen electrode (RHE), respectively. The electrolyte was an O_2-saturated aqueous solution of 0.1 M H_2SO_4. The RDE polarization curves were recorded with a scan rate of 10 $mV \cdot s^{-1}$ at 1500 rpm and corrected for the background current measured in N_2-saturated electrolyte. Additional measurements were similarly performed with a rotating-ring disk electrode for determination of the % H_2O_2 released during ORR. The ring potential was held at 1.2 V vs. RHE. Selected catalysts were investigated in fuel cell. For the membrane electrode assembly (MEA), cathode inks were prepared using the following formulation: 20 mg of catalyst, 652 μl of a 5 wt% Nafion solution containing 15–20% water, 326 μl of ethanol and 272 μl of de-ionized water. The inks were alternatively sonicated and agitated with a vortex mixer every 15 min, for a total of 1 h. Then, three aliquots of 405 μl of the catalyst ink were successively deposited on the microporous layer of an uncatalysed 4.84 cm^2 gas diffusion layer (Sigracet S10-BC) to reach a catalyst loading of 4 mg cm^{-2}. The cathode was then placed in a vacuum oven at 90°C to dry for 1 h. The anode used for all PEMFC tests performed in this work was 0.5 $mg_{Pt} \cdot cm^{-2}$ on Sigracet S10-BC. MEAs were prepared by hot-pressing 4.84 cm^2 anode and cathode against either side of a Nafion NRE-211 membrane at 125°C for 2 min. PEMFC tests were performed with a single-cell fuel cell with serpentine flow field (Fuel Cell Technologies Inc.) using an in-house fuel cell bench and a Biologic Potentiostat with a 50 A load and EC-Lab software. For the tests, the fuel cell temperature was 80°C, the humidifiers were set at 85°C, and the inlet pressures were set to 1 bar gauge for both anode and cathode sides. The flow rates for humidified H_2 and O_2 were ca 50–70 sccm downstream of the fuel cell. Polarization curves were recorded by scanning the cell voltage at 0.5 $mV \cdot s^{-1}$.

Results and Discussion

Structural characterisation of pristine catalysts.— The X-ray diffractograms for the pristine Fe-N-C, Co-N-C and Cr-N-C catalysts are shown in Figure 2. While the Fe-N-C and Co-N-C catalysts only show two diffraction peaks that are assigned to the 002 and 101 reflections of graphite, the Cr-N-C catalyst shows additional intense peaks that are assigned to the CrN structure. In addition, secondary peaks visible in the diffraction pattern of Cr-N-C are assigned to the Cr_2N structure and to a chromium carbonitride structure. The major presence of CrN over Cr_2N was expected after pyrolysis in the N-rich atmosphere, NH_3.[42] The superimposition of the broad peaks at 23–25° that is assigned to graphite highlights a similar low degree of graphitization. This is understandable since the metallic cobalt and iron crystalline structures known to catalyze graphitisation are not detected by XRD in the pristine Fe-N-C and Co-N-C catalysts while chromium nitrides do not catalyze graphitization.[29,43–44]

The Fourier-transforms of the extended X-ray absorption fine structure (EXAFS) spectra of the Fe-N-C and Co-N-C catalysts are shown in Fig. 3a–3b (thick solid lines), while the corresponding X-ray absorption near edge structure (XANES) spectra are shown in Fig. 3d–3e. The radial distribution function of Fe-N-C shows a first peak at 1.3–1.5 Å arising from Fe-N interactions and a second peak at 2.2 Å mostly assigned to backscattering from carbon atoms. Both the EXAFS and XANES spectra for pristine Fe-N-C resemble those of Fe(II) phthalocyanine ($Fe^{II}Pc$) (thin red line in Figs. 3a and 3d). The main difference is the absence of a pre-edge peak at 7117 eV in the XANES spectrum of Fe-N-C, while it is present in the spectrum of $Fe^{II}Pc$. The absence of the pre-edge feature in Fe-N-C can be explained on the basis that the square-planar D_{4h} local symmetry is broken down in the Fe-N-C catalyst due to the additional coordination of dioxygen along the axial direction.[45] The pre-edge feature at 7117 eV is indeed observed for square-planar $Fe^{II}N_4$ compounds but disappears for a square-pyramid coordination resulting from the coordination by a fifth ligand.[17,46] Such is the case for Hemin, a chloro-Fe(III)-porphyrin compound (green line in Fig. 3d). Thus, the XANES and EXAFS data for Fe-N-C show that i) the active-site structure in Fe-N-C is similar to that in $Fe^{II}Pc$ and ii) no or almost no Fe-Fe bonds exist in that catalyst. Similarly, the EXAFS data for Co-N-C suggest that only few Co-Co bonds are present in the pristine catalyst due to the small signal at 2.3–2.5 and 4–5 Å corresponding to

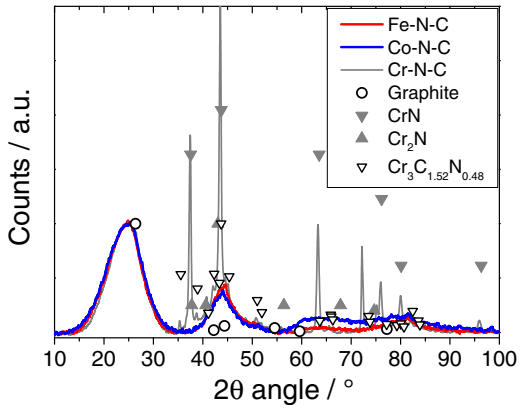

Figure 2. X-ray diffractograms of the pristine Fe-N-C, Co-N-C and Cr-N-C catalysts and reference X-ray diffraction lines for graphite (JCPDS file 75-1621), CrN (JCPDS file 11-0065), Cr_2N (JCPDS file 01-1232) and $Cr_3C_{1.52}N_{0.48}$ (JCPDS file 76-1037).

Author Proof

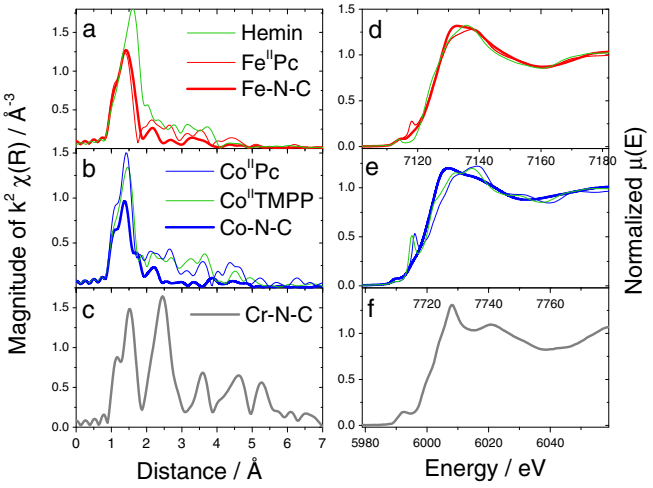

Figure 3. Left handside: Magnitude of the k^2-weighed Fourier transform of the EXAFS signal for the pristine Fe-N-C, Co-N-C and Cr-N-C catalysts and for reference compounds. The radial distance is not corrected for phase shift. Right handside: the corresponding normalized XANES spectra, at energies between −10 and +70 eV around the corresponding Metal K-edge.

Co-Co bond distances in metallic cobalt (thick blue line in Fig. 3b). On the basis of the relative intensity of the Fourier transform at 1.4 Å (Co-N interactions) for the present Co-N-C catalyst compared to that of a Co-based catalyst free of metallic cobalt particles (lower cobalt content), it was estimated that ca 79–83% of the cobalt atoms in the present Co-N-C catalyst are involved in CoN_xC_y moieties. Similar to the case for iron, the pre-edge feature is observed for the square-planar $Co^{II}N_4$ compounds Co^{II}Pc and Co(II)-tetramethoxyphenylporphyrin (Co^{II}TMPP) but not observed for Co-N-C (Fig. 3e). The active site structure in Co-N-C is also different from that in Co^{II}Pc or Co^{II}TMPP as revealed by the lower intensity of its Fourier transform at 1.4 Å, corresponding to Co-N interactions (Fig. 3b). This suggests a lower coordination of cobalt in Co-N-C than in CoN_4 macrocycles. In conclusion, the restricted amount of metal-based crystalline structures in the pristine Co- and Fe-N-C catalysts is important as it allows an easier tracking with X-ray absorption spectroscopy (XAS) of the fate of the CoN_xC_y and FeN_xC_y moieties after H_2O_2 treatment. This aspect had already proved important for *post mortem* Mössbauer analysis of Fe-N-C cathodes.[21] Last, the Fourier transform function for Cr-N-C shows a long-range ordering up to 6 Å, in agreement with the CrN structure. The first peak at 1.5 Å is assigned to Cr-N interactions with N atoms while the second and third peaks at 2.5 and 3.6 Å are assigned to Cr-Cr interactions.

Electrochemical characterization of pristine and degraded catalysts.— Figure 4 shows the polarization curves measured with RDE for the pristine Fe-N-C, Co-N-C and Cr-N-C catalysts (thick black curves) as well for the three series of catalysts obtained by treating these catalysts with increasing amounts of H_2O_2. The polarization curves for the pristine Fe- and Co-N-C catalysts show a gradual \transition from a kinetic control to a diffusion control extending over 150 mV. This is typical for catalytic films with poor diffusion properties. These experimental curves are similar in shape to those calculated for films including an O_2 concentration gradient at high current density.[47] This does however not impede the reading of the ORR activity at high potential where the current density is low. For both Fe- and Co-N-C, the ORR activity at 0.8 V vs. RHE gradually decreases with increasing amounts of H_2O_2 used during the treatment, while the diffusion-limited current density is practically unmodified. This suggests that the ORR mechanism was unchanged while the number of FeN_xC_y and CoN_xC_y active sites on the surface gradually decreased. The general trend of decreasing ORR activity with increased amount of H_2O_2 used in the treatment is however more

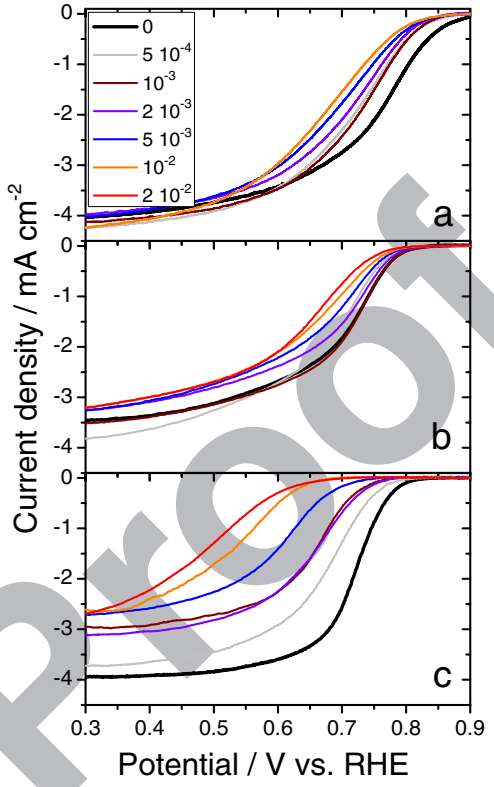

Figure 4. Polarization curves measured with RDE for a) Fe-N-C, b) Co-N-C and c) Cr-N-C pristine catalysts and after ex situ treatment with various amounts of H_2O_2. The legend indicates the number of moles H_2O_2 per mg of catalyst used for treating Me-N-C catalysts.

complex at low peroxide amounts. For Fe-N-C, the ORR activities after treatment with $5 \cdot 10^{-4}$ and 10^{-3} mol H_2O_2 per mg of catalyst are identical, suggesting that the degradation stalled. For Co-N-C, the ORR activity first decreased after treatment with $5 \cdot 10^{-4}$ mol H_2O_2 per mg of catalyst, but rose back to the activity of pristine Co-N-C after treatment with 10^{-3} mol H_2O_2 mg^{-1}. For higher amounts of H_2O_2, the ORR activity then decreased gradually for both Fe- and Co-N-C. The H_2O_2 treatment seems to result in the superimposition of a minor positive effect at low H_2O_2 amount and of a major negative effect at high H_2O_2 amount. Following a restricted surface oxidation with H_2O_2, the top surface of Co- or Fe-N-C might have been cleaned, thereby exposing to the electrolyte some active sites that were previously buried under a thin carbon layer. Alternatively, the grafting of oxygen groups on the surface might have positively affected the ORR turnover of the active sites via electronic effects.[48] Next, the pattern for Cr-N-C is different. The polarization curve of the pristine catalyst is steeper in the kinetic region. The diffusion-limited current density is also better defined. The decrease of the ORR activity after H_2O_2 treatment is much larger than that observed for Fe- and Co-N-C. This suggests that the nature of the active sites is completely different, which is corroborated by XRD, XANES and EXAFS characterisations (Figs. 2–3). As will be seen later, the chromium nitride structures resist the peroxide treatment, but they are ORR inactive. The ORR activity of pristine Cr-N-C is assigned to highly basic N-groups that are formed during pyrolysis in NH_3. The assignment is based on the poor ORR activity of a Cr-based sample pyrolyzed in Ar and also on the high activity of a metal-free N-C sample pyrolyzed in NH_3 (not shown). Regarding the diffusion-limited current density, the pattern is also very different from that observed for Fe- and Co-N-C. The ORR mechanism seems to gradually shift from a four-electron to a two-electron reduction mechanism (Fig. 4c). This is understandable if the top-surface N-groups present in pristine Cr-N-C were removed from the surface during the treatment with H_2O_2, or chemically

Author Proof

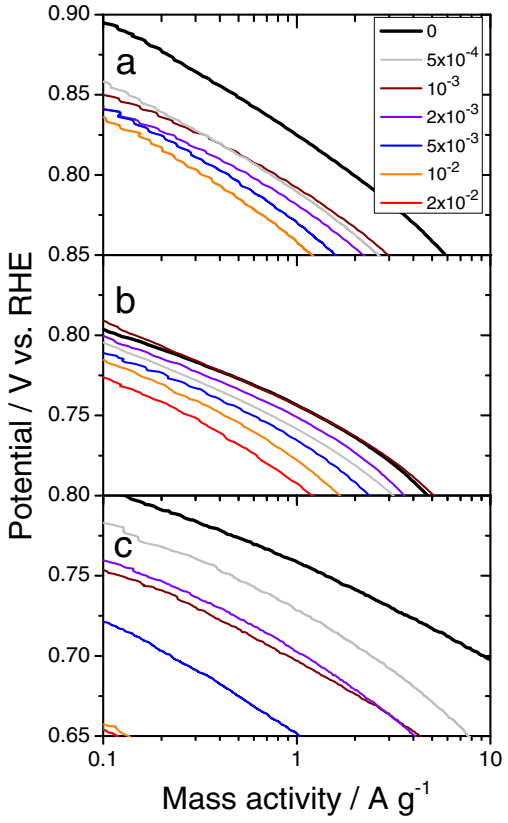

Figure 5. Tafel plots derived from RDE polarization curves for a) Fe-N-C, b) Co-N-C and c) Cr-N-C catalysts initially and after ex situ treatment with various amounts of H_2O_2. The legend indicates the number of moles H_2O_2 per mg of catalyst used to treat Me-N-C catalysts.

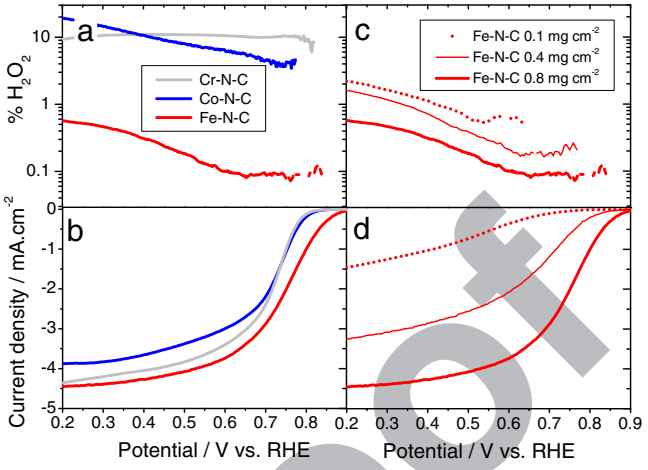

Figure 6. Rotating ring disk electrode measurements for Fe-N-C, Co-N-C and Cr-N-C (left handside) at a fixed loading of 0.8 mg cm^{-2} and rotating ring disk electrode measurements for Fe-N-C at different loading (right handside). In c and d, the loading at the disk was 0.8 mg cm^{-2} (thick solid line), 0.4 mg cm^{-2} (thin solid line) or 0.1 mg cm^{-2} (dashed line).

modified. The low ORR activity remaining after extensive degradation with H_2O_2 possibly comes from less active N-groups or from oxygen groups that formed during the peroxide treatment. In order to quantify the ORR activity, the polarization curves were corrected for diffusion limitation with the Koutecky-Levich equation and normalized per mass of catalyst. Figure 5 shows the Tafel plots corresponding to Figure 4. Within a given catalyst series, the Tafel slopes remained constant with H_2O_2 treatment, except for pristine Fe-N-C for which the Tafel slope is slightly higher than that for treated catalysts (77 vs. 62–65 mV dec^{-1}). The ORR activity after treatment with 10^{-2} mol H_2O_2 mg^{-1} was divided by 6.6 for Fe-N-C, 2.9 for Co-N-C and 1400 for Cr-N-C (Fig. 5). The activity was read at 0.8 V vs. RHE for Fe- and Co-N-C, and at 0.75 V vs. RHE for Cr-N-C. Thus, the ORR activity decay following H_2O_2 treatment strongly depends on the nature of the metal in Me-N-C catalysts. This in turn strongly suggests that the oxidizing species degrading the catalysts is not H_2O_2 but rather the ROS generated via a Fenton reaction between transition metal atoms and H_2O_2. Direct evidence for the formation of ROS is reported in Collection yield and radical oxygen species after ex situ H_2O_2 treatment section.

The ORR mechanism on pristine catalysts was then investigated with a rotating ring disk electrode (RRDE). Measured at a loading of 0.8 mg cm^{-2}, the % H_2O_2 detected at the ring is shown in Fig. 6a and the polarization curves measured at the disk are shown in Fig. 6b. The % H_2O_2 is far lower for ORR when catalyzed by Fe-N-C than catalyzed by Co-N-C and Cr-N-C. The curves of % H_2O_2 vs. potential for Fe-N-C and Co-N-C have a similar shape, but Co-N-C produces ca 20 times more H_2O_2 at any given potential. For Cr-N-C, the % H_2O_2 is quite high and almost independent of potential. In order to investigate whether the low % H_2O_2 measured on Fe-N-C indicates a true four electron reduction mechanism, a 2 + 2 electron mechanism or a two-electron mechanism followed by chemical disproportionation, lower Fe-N-C loadings were investigated (Fig. 6c–6d).[49] At lower loadings, the diffusion-limited current density was drastically reduced (Fig. 6d), due to incomplete coverage of the disk, or due to a low density of active sites per geometric area of the disk. This drastic decrease does not reflect the small change in % H_2O_2 that is detected at the ring. The % H_2O_2 increased with decreased loading, but remained in the range 3.3–4.5% at potentials of 0.2–0.6 V vs. RHE even at 0.1 $mg_{Fe\text{-}N\text{-}C}$ cm^{-2} (dashed curve in Fig. 6d). This shows that ORR on Fe-N-C proceeds mostly according to a direct four electron mechanism. The minute amount of H_2O_2 formed on the catalyst surface may however have formed ROS through a chemical reaction on FeN_xC_y moieties.

While the RDE and RRDE techniques are useful for investigating the ORR activity and ORR mechanism, they do not allow predicting the behavior of Me-N-C cathodes at high current density in PEMFC. We selected the pristine catalysts and catalysts treated with $2 \cdot 10^{-3}$ and 10^{-2} mol H_2O_2 mg^{-1} for beginning-of-life (BoL) PEMFC tests. Figure 7 shows PEMFC polarization curves recorded with 4 mg cm^{-2} of Me-N-C catalyst at the cathode. Analyzing the extent of degradation after ex situ H_2O_2 treatment should a priori be carried out by comparing the BoL polarisation curve of H_2O_2-treated catalysts to the BoL polarization curves of the corresponding pristine catalysts. However, for the pristine Fe- and Co-N-C catalysts, this simple approach is impeded by the fact that the BoL polarization curve does not correspond to the best performance of the pristine catalysts. For pristine Fe-N-C, the polarization curve continuously improves during the first 6 h of operation, and the same occurs for pristine Co-N-C during the first 15 h of operation. The improvement is most visible in the high current density region, while the ORR activity at high potential slightly decreases during this break-in period (Fig. 7a–7b). The break-in phenomenon is assigned to changes in the hydrophilic properties of the catalytic surface that had never been in contact with water previously. This break-in period is neither observed for pristine Cr-N-C nor for any H_2O_2-treated catalyst. When the high current density region is considered, the reference curves for the pristine Fe-N-C and Co-N-C catalysts will therefore be the polarisation curves after break-in (dotted black lines in Fig. 7a–7b). When the ORR activity at 0.8 V is considered, the reference curves for the pristine Fe-N-C and Co-N-C catalysts will be the BoL polarization curves (solid black lines in Fig. 7a–7b). The current densities measured at 0.8 and 0.5 V in fuel cell as extracted from Fig. 7 for pristine and H_2O_2-treated catalysts are summarized in Figure 8.

Author Proof

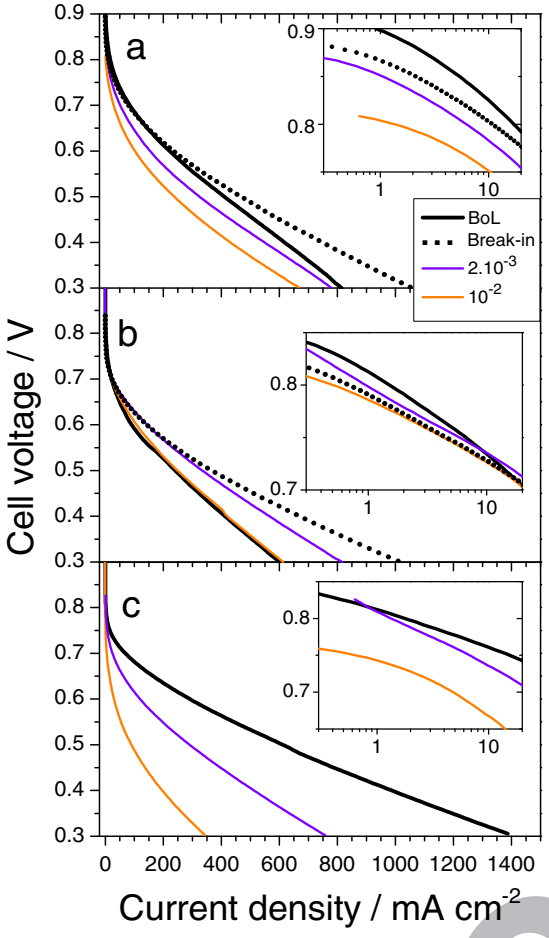

Figure 7. Effect of ex situ H_2O_2 treatment on the fuel cell polarization curves of MEAs with cathodes comprising a) Fe-N-C, b) Co-N-C and c) Cr-N-C catalysts. The insets show the high-potential region of the polarization curves in semi-logarithmic plot. The break–in involved potentiostatic control at 0.5 V for 6 h (pristine Fe-N-C) or 15 h (pristine Co-N-C).

As previously observed with RDE, the degradation of the cathode performance after treating the catalysts with 10^{-2} mol H_2O_2 mg^{-1} is most severe for Cr-N-C, followed by Fe-N-C and then Co-N-C. After a treatment with 10^{-2} mol H_2O_2 mg^{-1}, the ORR activity measured in PEMFC at 0.8 V was divided by ca 45 for Cr-N-C, by 9 for Fe-N-C and by 3 for Co-N-C (Fig. 8b). These numbers are comparable to those measured with RDE, except for Cr-N-C for which the decay in fuel cell is much smaller than the one measured in RDE (Fig. 5c and 7c). At 0.5 V, the decrease in current density from the BoL polarization curve (Cr-N-C), or from the polarisation curve after break-in (for Co- and Fe-N-C) to the BoL polarisation curve measured for catalysts treated with 10^{-2} mol H_2O_2 mg^{-1} is highest for Cr-N-C (decrease from 606 to 85 mA cm^{-2}), followed by Fe-N-C (470 to 238 mA cm^{-2}) and smallest for Co-N-C (366 to 240 mA cm^{-2}). Noteworthy, the ORR activity at 0.8 V is almost identical for the pristine Co-N-C catalyst after break-in and for the Co-N-C catalyst after treatment with 10^{-2} mol H_2O_2 mg^{-1} (Fig. 8b). In spite of this, a large difference is observed in the current density at 0.5 V (Fig. 8a). Thus, for Co-N-C, the loss of performance at high current density induced by the peroxide treatment is mostly due to decreased transport properties of the cathode layer. The story is different for Fe-N-C and Cr-N-C. The Fe-N-C catalyst shows a stronger decay of its ORR activity after peroxide treatment (Fig. 8b) but the transport properties of the cathode layer are also negatively impacted by the ex situ peroxide treatment of the catalyst, as can be deduced from the steeper slope of the polarization curve at high current density (Fig. 7a). The Cr-N-C based cathode shows a

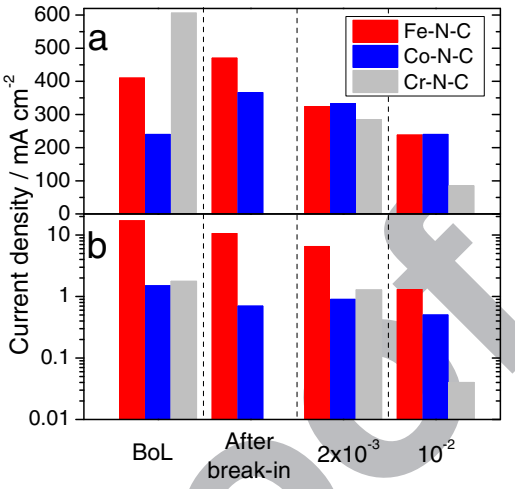

Figure 8. Current density measured in PEMFC at 0.5 V (a) and 0.8 V (b) for the pristine catalysts at BoL or after break-in, and for the catalysts after treatment with $2{\cdot}10^{-3}$ or 10^{-2} mol H_2O_2 mg^{-1}. The break–in involved potentiostatic control at 0.5 V for 6 h (pristine Fe-N-C) or 15 h (pristine Co-N-C). No break-in was applied to Cr-N-C. The activity of Cr-N-C at 0.8 V after 10^{-2} mol H_2O_2 mg^{-1} needed an extrapolation.

dramatic decrease of both its ORR activity and transport properties due to the H_2O_2 ex situ treatment of the Cr-N-C catalyst (Fig. 8, gray columns).

Collection yield and radical oxygen species after ex situ H_2O_2 treatment.— The weight percentage of catalyst powder collected after each H_2O_2 treatment is reported in Fig. 9a. After a treatment with $5{\cdot}10^{-4}$ to $5{\cdot}10^{-3}$ mol H_2O_2 mg^{-1}, the collection yields are 87–90% for Fe-N-C (red bars) and 77–85% for Cr-N-C (gray bars). Collection yields lower than 100% can be due to i) handling loss, ii) chemical loss due to the oxidative attack by peroxide and ii) filtration loss. The latter occurs if, at the end of the treatment, some catalytic particles are smaller than the pore size of the filter used to separate the treated

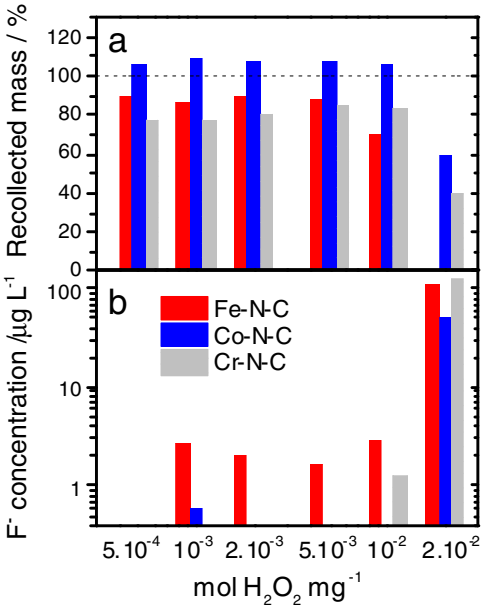

Figure 9. Extent of the H_2O_2 ex situ degradation assessed a) with the relative mass of catalyst recollected after each H_2O_2 treatment + filtration + drying, or b) with the concentration in the filtrate of fluoride ions released by a Nafion membrane.

Author Proof

catalyst from the solution. The non-collected mass of catalyst for the treated Fe-N-C and Cr-N-C samples is mostly assigned to chemical and filtration losses. The loss due to material's handling is believed to be negligible since for Co-N-C samples handled similarly, a weight gain was observed after treatment up to 10^{-2} mol H_2O_2 mg^{-1} (blue bars in Fig. 9a). This weight gain is assigned to the grafting of oxygen functionalities on the surface of Co-N-C, without any loss of carbon atoms from Co-N-C. This explanation is supported by XPS elemental analysis (III.6). The lower collection yields for Cr-N-C samples than for Fe-N-C samples is assigned to the higher porosity and higher specific area of the pristine Cr-N-C catalyst due to the ammonia gas used during pyrolysis. A significant decrease of the collection yield is observed at and above 10^{-2} mol H_2O_2 mg^{-1}. After treatment with $2 \cdot 10^{-2}$ mol H_2O_2 mg^{-1}, only 60 and 40% of the initial Co-N-C and Cr-N-C mass was collected whereas no Fe-N-C catalyst could be collected on the filter. A large fraction of the missing mass of catalyst is suspected to have passed through the 220 nm sized pores of the filter as a consequence of finer powders following the H_2O_2 treatment. This hypothesis is supported by the greyish color of the filtrates after treatment with large amounts of peroxide. The lower granulometry of the powders after extended treatment with peroxide may explain the poorer transport properties of fuel cell cathodes (Fig. 7). The cathode macroporosity may have decreased due to a lower 3D branching character and lower inter-particle connections for H_2O_2-treated catalysts. In conclusion, after treatment with 10^{-2} mol H_2O_2 mg^{-1}, the extent of catalyst modification clearly depends on the nature of the transition metal in Me-N-C catalysts, in the order Fe > Cr > Co. This, in turn, might be related to the production of ROS ensuing from the reaction between H_2O_2 and metal species. The production of ROS during the peroxide treatment was quantified with the concentration of fluoride ions measured in the filtrate at the end of each treatment. These fluoride ions originate from the simultaneous attack by ROS of the Nafion membrane immersed in the solution during the entire process. While the fluoride concentration remained low after treatment up to 5.10^{-3} mol H_2O_2 mg^{-1}, it dramatically increased by ca two orders of magnitude for all three catalysts after a treatment with $2 \cdot 10^{-2}$ mol H_2O_2 mg^{-1} (Fig. 9b). A correlation is observed between a high collection yield and a low concentration of fluoride, suggesting that Co-N-C produces less ROS than Fe-N-C when it is contacted by H_2O_2. This explains the restricted decrease of the electrochemical performance of Co-N-C after H_2O_2 treatment.

X-ray absorption spectroscopy on pristine and degraded catalysts.— The XANES spectra for the three series of H_2O_2 treated catalysts are shown in Fig. 10. For Fe-N-C, there is practically no change of the XANES spectra from the pristine Fe-N-C catalyst up to the highly degraded catalyst after treatment with 10^{-2} mol H_2O_2 mg^{-1} (Fig. 10a). Also the Fourier-transforms of the EXAFS spectra of the Fe-N-C samples did not reveal any changes and were identical to that of pristine Fe-N-C shown in Fig. 3a. The XANES and EXAFS spectra of the Fe-based series therefore demonstrate that the coordination chemistry of the Fe atoms that remained in the samples after H_2O_2 treatment is identical to the one before treatment. It is paramount to realize that this observation does not preclude the possibility that the FeN_xC_y moieties located on the top-surface in pristine Fe-N-C were partially or fully removed during H_2O_2 treatment. If similar FeN_xC_y moieties are present both on the top surface and in the bulk of pristine Fe-N-C, the normalized XANES and EXAFS spectra will remain unchanged even after the complete removal of top surface sites due to the bulk-averaging nature of XANES and EXAFS. Hence, identical spectra before and after H_2O_2 treatment is not paradoxical with the decreased ORR activity before and after H_2O_2 treatment. It strongly suggests, however, that only a fraction of the FeN_xC_y moieties existing in pristine Fe-N-C were located on the top surface. Only the latter may contribute to the ORR activity. For the series of H_2O_2-treated samples derived from pristine Co-N-C, the XANES spectra changed noticeably with H_2O_2 treatment (Fig. 10b). The inset in Fig. 10b shows the initial increase of the white line intensity at ca 7726 eV after treatment with $5 \cdot 10^{-4}$ and 10^{-3} mol H_2O_2 mg^{-1}, followed by a continuous decrease from 10^{-3} to $2{\cdot}10^{-2}$ mol H_2O_2 mg^{-1}. Noteworthy, after treatment with 10^{-3} mol H_2O_2 mg^{-1}, the ORR activity measured in RDE increased back to the ORR activity of pristine Co-N-C, and these two observations might be interrelated. The two XANES spectra corresponding to treatments with 10^{-2} and $2{\cdot}10^{-2}$ mol H_2O_2 mg^{-1} are significantly different at 7726 eV and are also negatively shifted by 1.5–2.5 eV at the beginning of the absorption edge (7715 eV). This indicates a decreased average oxidation state of cobalt. This observation is further supported by the Fourier-transforms of the EXAFS signal, showing an increased peak at ca 2.2, 3.8 and 4.5 Å (Fig. 11). These distances (not corrected for phase shift) correspond to back-scattering from cobalt atoms in metallic cobalt. Extensive treatment with H_2O_2 probably resulted in the etching of a significant fraction of the CoN_xC_y moieties present in pristine Co-N-C, thereby increasing the fraction of

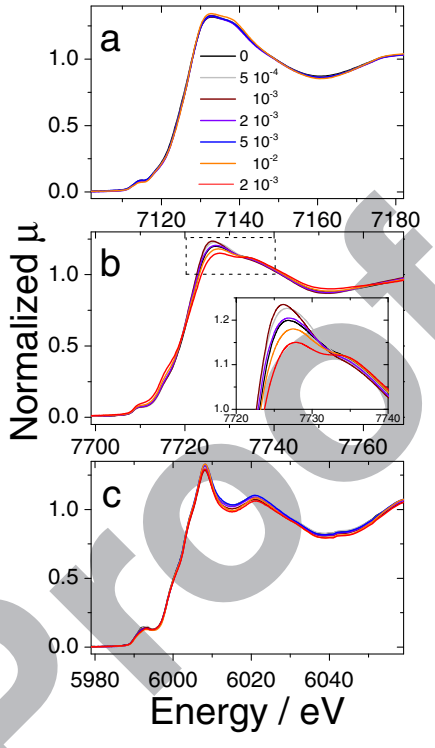

Figure 10. Normalized XANES spectra for pristine and H_2O_2 treated catalysts. a) Fe-N-C, b) Co-N-C, c) Cr-N-C. The spectra are shown in the energy range −10 to +70 eV around the corresponding Metal K-edge.

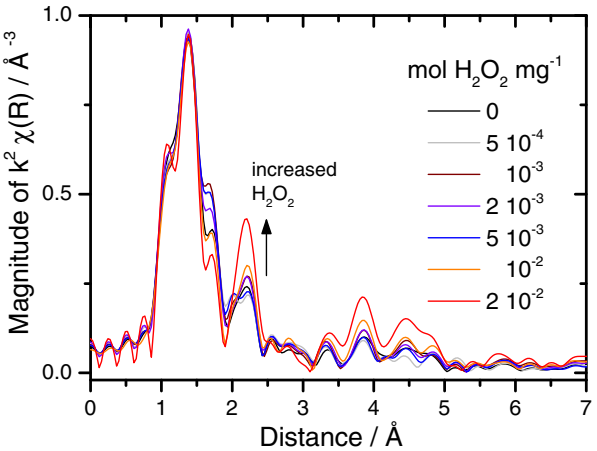

Figure 11. Magnitude of the k^2-weighed Fourier transform of the EXAFS signal for pristine Co-N-C and for H_2O_2 treated Co-N-C. The radial distance is not corrected for phase shift.

Author Proof

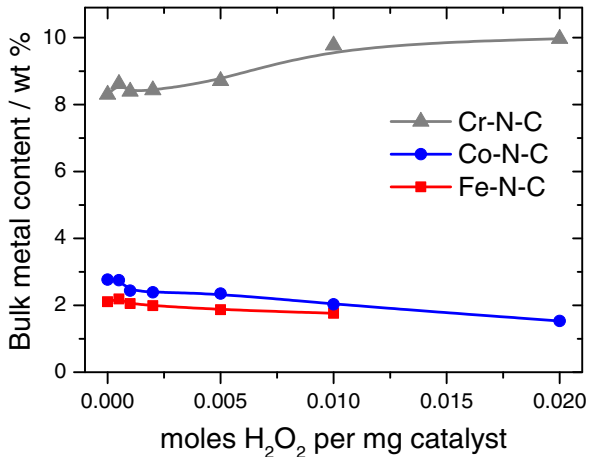

Figure 12. Bulk metal content as a function of the ratio of mol H_2O_2 per mass catalyst used for ex situ degradation.

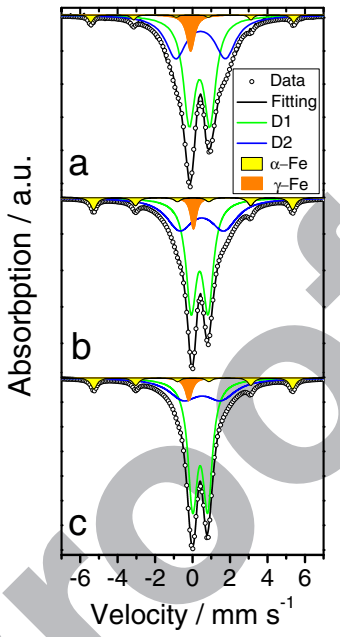

Figure 13. Mössbauer absorption spectra measured for pristine Fe-N-C and after ex situ treatment with H_2O_2. a) pristine, b) after $2 \cdot 10^{-3}$ mol H_2O_2 mg^{-1}, c) after 10^{-2} mol H_2O_2 mg^{-1}.

metallic cobalt in the treated Co-N-C samples. Pristine Co-N-C seems to contain a small fraction of metallic cobalt (Fig. 11), although it was not detected by XRD (Fig. 2). The better resistance of metallic cobalt particles to the peroxide treatment is normal since such particles are usually surrounded by a continuous layer of graphitic carbon after pyrolysis. Next, the XANES spectra for the pristine and treated Cr-N-C catalysts show little change with H_2O_2 treatments (Fig. 10c). This agrees with the known stability of chromium nitride structures.

In addition to providing knowledge on the oxidation state and coordination chemistry of transition metals, XAS allows quantifying the bulk metal content from the absolute height of the absorption step combined with the exact mass of each pellet used for measurements in transmission mode. Figure 12 shows the bulk content of Fe, Co and Cr determined from XAS as a function of the number of mol H_2O_2 used to treat the catalysts. The bulk contents of Fe and Co decreased with increasing amounts of H_2O_2. However, the loss is moderate. After a treatment with 10^{-2} mol H_2O_2 mg^{-1}, the relative decrease of Fe and Co content was only 17 and 27%, respectively. For Cr-N-C, the bulk metal content even increased by 18%, highlighting the better resistance to the peroxide treatment of CrN particles than the N-doped carbon matrix. Dodelet's group also reported in 2003 a relative loss of Fe of only 30–40% after H_2O_2 treatment. In parallel, the half-wave potential for ORR in RDE decreased by 150–200 mV, corresponding to ca two-order-of-magnitude decrease in ORR activity.[25] For another Fe-N-C catalyst, Zelenay's group observed a decrease of Fe content from 0.9 to 0.6 at. % (33% relative los) after H_2O_2 treatment for 72 h, which was accompanied by a 150 mV downshift of the half-wave potential for ORR when measured in RDE.[26] A XANES analysis with linear combination fitting of reference spectra identified that only 20–25% of the iron atoms in their pristine catalyst were involved in a $Fe^{II}Pc$-like coordination, the remainder being iron sulfide, iron oxide and metallic iron structures. This complicated the identification of a correlation, or lack of correlation, between the decrease in bulk content of FeN_xC_y moieties during H_2O_2 treatment and the decrease of ORR activity. Here in contrast, ca 80 and 90% of the metal atoms in the pristine Co-N-C and Fe-N-C catalysts are assigned to MeN_xC_y moieties, respectively (see Structural characterisation of pristine catalysts section and ^{57}Fe Mössbauer spectroscopy on pristine and degraded Fe-N-C catalysts section). The relative loss of only 27 and 17% of Co and Fe compared to the ORR activity loss measured in RDE after a treatment with 10^{-2} mol H_2O_2 mg^{-1} (activity divided by a factor 6.6 for Fe-N-C and 2.9 for Co-N-C) suggests that only a fraction of the Fe and Co atoms in the pristine catalysts are located on the top surface and participate in the ORR. Alternatively, if a major fraction of MeN_xC_y moieties is located on the top surface initially, the results suggest that surface oxidation due to H_2O_2 drastically reduced the turnover frequency for ORR of the remaining MeN_xC_y moieties. In this second hypothesis, the fact that little or no modification of the XANES spectra is observed after H_2O_2 treatment, especially for Fe-N-C, suggests that the oxidation would have mostly occurred on the N-doped carbon matrix. Preferential oxidation at the edge of graphene sheets could have modified the electronic properties. The latter might in turn have modified the access of electrons to the MeN_xC_y moieties. The latter are believed to be covalently integrated near the edge, or at the edge, of graphene sheets.[48,50–55] Decreased electronic properties and conductivity at the edge would have profound implications in particular for MeN_xC_y moieties located in micropores.[56,57]

^{57}Fe Mössbauer spectroscopy on pristine and degraded Fe-N-C catalysts.— Mössbauer spectroscopy is a powerful technique to identify the presence of different iron coordinations in multiphase materials. It is therefore ideally suited to be used alone or in combination with XAS.[58–60] With EXAFS, the secondary peak observed at ca 2.1–2.3 Å in the Fourier-transform may be assigned to backscattering from either carbon atoms in the second coordination sphere of FeN_xC_y moieties, or from iron atoms in the first or second coordination sphere of metallic iron or iron carbide (Fig. 3a). The detection of a minor fraction of iron atoms involved in Fe-based crystalline structures is therefore difficult with EXAFS. Figure 13 shows the ^{57}Fe Mössbauer spectra for pristine Fe-N-C and for samples obtained after its treatment with $2 \cdot 10^{-3}$ and 10^{-2} mol H_2O_2 mg^{-1}. The Mössbauer spectrum of pristine Fe-N-C shows that the major components are the doublets D1 and D2 (Fig. 13a). They have previously been assigned to a square-planar $Fe^{II}N_4$ coordination with Fe^{II} in low and medium spin, respectively.[58–61] Doublets D1 has Mössbauer parameters similar to those of unpyrolyzed $Fe^{II}Pc$ adsorbed on carbon, while D2 has parameters similar to those of crystalline $Fe^{II}Pc$ in which stacked molecules interact with each other (Table I).[62] A sextet and a singlet component are also detected and unambiguously assigned to α-Fe and γ-Fe, respectively (Fig. 13a).[63] The spectral areas of these two components represent only 10% (Table I), demonstrating that the major fraction of iron atoms in pristine Fe-N-C is engaged in molecular-like FeN_xC_y moieties. Figures 13b and 13c show the spectra after peroxide treatment with $2 \cdot 10^{-3}$ and 10^{-2} mol H_2O_2 mg^{-1}, respectively. No major changes are observed. With increasing amount of H_2O_2, a trend of increased relative fraction of D1 and decreased relative fraction of D2 is noticed. In parallel, the relative fraction summed for α-Fe

Author Proof

Table I. Mössbauer parameters derived from the fitting with four components of the spectrum for pristine Fe-N-C and for Fe-N-C after ex situ treatment with $2 \cdot 10^{-3}$ and 10^{-2} mol H_2O_2 mg^{-1}. The hyperfine field of the sextet was 33.6, 33.0 and 32.9 T for pristine Fe-N-C, $2 \cdot 10^{-3}$ and 10^{-2} treated Fe-N-C samples, respectively.

	Relative Area/%			Isomer Shift/mm s^{-1}			Quadrupole Splitting/mm s^{-1}			
	Pristine	$2 \cdot 10^{-3}$	10^{-2}	Pristine	$2 \cdot 10^{-3}$	10^{-2}	Pristine	$2 \cdot 10^{-3}$	10^{-2}	Assignment
D1	53 ± 5	51 ± 2	59 ± 3	0.38 ± 0.01	0.38 ± 0.00	0.40 ± 0.00	1.10 ± 0.02	0.90 ± 0.01	0.80 ± 0.01	$Fe^{II}N_4/C$, LS
D2	38 ± 3	37 ± 2	29 ± 2	0.43 ± 0.02	0.49 ± 0.01	0.51 ± 0.02	2.65 ± 0.08	2.36 ± 0.06	2.01 ± 0.13	$Fe^{II}N_4/C$, MS
Sextet	3 ± 1	7 ± 0	7 ± 0	-0.02 ± 0.03	0.03 ± 0.01	0.04 ± 0.01	–	–	–	α-Fe
Singlet	6 ± 1	4 ± 0	4 ± 0	-0.10 fixed	0.05 ± 0.01	-0.20 ± 0.01	–	–	–	γ-Fe

and γ-Fe increases only from 9 to 11%. Such metallic particles are embedded in a graphitic shell and resist oxidative attacks, as previously shown in a high-voltage degradation study of the same catalyst.[21] If a large amount of FeN_xC_y moieties had been removed from the catalyst during H_2O_2 treatment, the relative fraction of α-Fe and γ-Fe after treatment would have dramatically increased. The fact that it only increased from 9 to 11% (+22% relative increase) confirms that most of the FeN_xC_y moieties existing in pristine Fe-N-C are still present after treatment with 10^{-2} mol H_2O_2 mg^{-1}. This agrees with the moderate decrease in bulk Fe content, only 17% relative decrease after treatment with 10^{-2} mol H_2O_2 mg^{-1} (Fig. 12). Due to the trends of relative area of D1 and D2, it can be concluded that the peroxide treatment preferentially removed FeN_xC_y moieties assigned to D2. The relative loss of 17% Fe after treatment with 10^{-2} mol H_2O_2 mg^{-1} can however not entirely be assigned to the removal of D2 sites. If this were true, the decrease in the relative area of D2 would have been commensurate with that number. However, it only decreased from 38 to 29% (Table I). Hence, the H_2O_2 treatment etched a minor fraction of both the D2 and D1 sites that were initially present in pristine Fe-N-C. These fractions can be estimated mathematically. If one considers 100 Fe atoms in pristine Fe-N-C, then 53 Fe atoms are in D1 sites, 38 atoms in D2 sites and the remainder in metallic structures (Table I). The H_2O_2 treatment with 10^{-2} mol H_2O_2 mg^{-1} removed 17 out of those 100 atoms (17% loss). After trial-and-error calculations, it is found that when, among those 17 Fe atoms, 4 come from D1 sites, 13 from D2 sites and none from the metallic structures, then the final relative % of D1 and D2 in the H_2O_2 treated sample are $100 \times (53\text{-}4)/(100\text{-}17) = 59\%$, and $100 \times (38\text{-}13)/(100\text{-}17) = 30\%$. These percentages match those experimentally observed for D1 and D2 after treatment with 10^{-2} mol H_2O_2 mg^{-1} (Table I, column 4). The decrease in the absolute content of Fe atoms involved in D1 and D2 coordinations upon treatment with 10^{-2} mol H_2O_2 mg^{-1} can now be calculated. It is ca $100 \times 4/53 = 7.5\%$ for D1, and $100 \times 13/38 = 34\%$ for D2. This information is more precise than the overall loss of 17% Fe obtained from XAS. Nevertheless, no proportional relationship can be drawn with the decrease in ORR activity for Fe-N-C. After treatment with 10^{-2} mol H_2O_2 mg^{-1}, the latter was divided by 6.6 and by 9 in RDE and PEMFC measurements, respectively (Electrochemical characterization of pristine and degraded catalysts section).

In conclusion, Mössbauer spectroscopy reveals that most of the FeN_xC_y moieties present in pristine Fe-N-C survived the peroxide treatment. The Mössbauer parameters of D1 and D2 were only slightly modified, especially for D1. This suggests that the active sites remaining in the peroxide-treated catalysts have an electronic structure and coordination chemistry very similar to those in the pristine catalyst. The apparent continuous decrease of the QS values for D1 and D2 with increased mol H_2O_2 mg^{-1} used for ex situ degradation might be due to electronic effects of the surrounding carbon support, which becomes more oxidized and contains fewer delocalized π electrons. Hence, either the ORR activity in pristine Fe-N-C is due to a minor fraction of D1 or D2 sites located on the top surface, or the top surface of the catalyst was highly oxidized during H_2O_2 treatment, leading to a loss of surface conductivity or partial exfoliation of the graphene sheets. The latter transformations may be localized around the surface FeN_xC_y moieties, where H_2O_2 reacted to form ROS.

X-ray photoelectron spectroscopy on pristine and degraded catalysts.— The nitrogen and oxygen content and speciation were investigated with XPS on pristine catalysts as well as on catalysts after treatment with 10^{-2} mol H_2O_2 mg^{-1}. Figure 14 shows as an example the N_{1s} narrow scan spectra for the pristine and degraded Fe-N-C catalyst. Both experimental spectra were fitted with four components (Table II). They are assigned in the order of increasing binding energy (BE) to pyridinic, pyrrolic, graphitic and oxidized nitrogen.[64–67] The pyridinic component (BE 398.5-398.7), primarily assigned to N atoms contributing with one electron to the π system, may also comprise N atoms ligating the Fe or Co ions.[66–67] Next, most pyrrolic N atoms are expected to be located on the graphene edges, and bonded to two C atoms and 1 H atom in six-membered rings. Third, the graphitic N component comprises all N atoms bonded with three C-atoms, either within a graphene sheet or at the edge of a graphene sheet.[64,68]

From Fig. 14, it can be seen that no novel N-species arose during the treatment of Fe-N-C with H_2O_2. This observation holds for Co-N-C and Cr-N-C. The modified shape of the overall N_{1s} spectrum in Fe-N-C after degradation is due to a larger relative fraction of pyrrolic-N. After quantification of the atomic % of C, N and O, it is found that the absolute content of pyrrolic N increased from 1.07 to 1.97 at % during degradation, (Table II). This absolute increase in pyrrolic N is also observed with Co-N-C and Cr-N-C (Table II). In contrast, the absolute content of all other N species in Fe-N-C, Co-N-C or Cr-N-C was unmodified or increased only slightly after H_2O_2 treatment. The exception is the significant decrease of pyridinic N for Cr-N-C after H_2O_2 degradation (ca -1 at %). The changes observed in the nitrogen

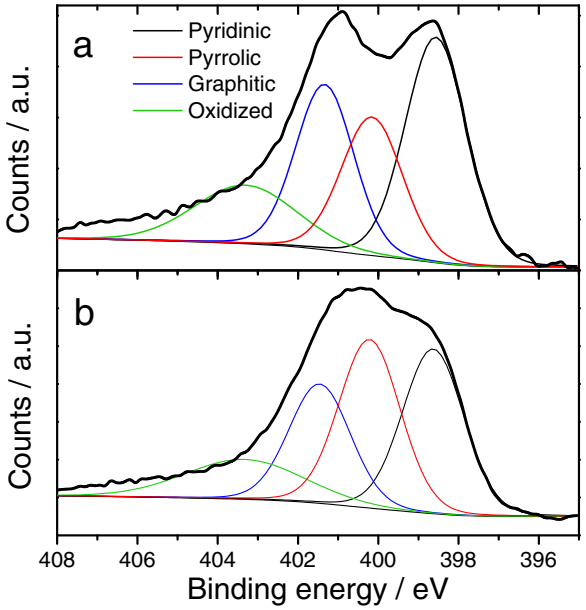

Figure 14. N_{1s} narrow scan spectra measured with XPS for a) the pristine Fe-N-C catalyst and b) the Fe-N-C catalyst treated with 10^{-2} mol H_2O_2 mg^{-1}. The experimental spectra were fitted with four nitrogen components.

Author Proof

Table II. X-ray photoelectron spectroscopy analysis of the N_{1s} and O_{1s} narrow scans for pristine catalysts and catalysts degraded with 10^{-2} mol H_2O_2 mg^{-1}. For Cr-N-C, a fifth N-component at 396.5–396.7 eV assigned to CrN was present with 0.15 and 0.33 atom % in the pristine and degraded catalysts, respectively.

	Nitrogen					Oxygen				
	Pyridinic or MeN_x	Pyrrolic	Graphitc	Oxidized	Total	O1	O2	O3	O4	Total
BE range/eV	398.5–398.7	400.0–400.4	401.3–401.5	403.3–403.7		530.8–531.2	532.5–532.8	534.2–534.3	536.2–536.7	
Fe-N-C pristine	1.75	1.07	1.21	0.76	4.8	1.14	2.64	0.70	0.12	4.6
Fe-N-C degraded	1.93	1.97	1.40	0.90	6.2	4.20	6.55	1.50	0.55	12.8
Co-N-C pristine	1.76	0.84	1.55	0.85	5.0	1.81	2.79	0.47	0.13	5.2
Co-N-C degraded	2.20	1.46	1.54	0.90	6.1	2.79	5.40	1.00	0.32	9.5
Cr-N-C pristine	3.08	1.25	1.43	0.79	6.7	3.54	2.79	0.48	0.39	7.2
Cr-N-C degraded	2.02	2.10	1.28	0.57	6.3	5.11	6.22	1.23	0.93	13.5

speciation for Fe-N-C and Co-N-C are now discussed in parallel, due to their similar active site structure. As a result of increased pyrrolic N and unmodified content of other N-species, the absolute N content increased by 1.1–1.4 at % after the peroxide treatment of Fe-N-C and Co-N-C (Table II). This is counter-intuitive. The least stable carbon atoms must have been substituted by nitrogen atoms from N_2 in air, a substitution that might have been catalyzed by ROS. Increased content of nitrogen was previously observed by Zelenay's group after ex situ H_2O_2 treatment of another Fe-N-C catalyst.[26] In that study, after a sharp drop from 6 to 3 at % N after 24 h of immersion in a 10% H_2O_2 solution (unmodified ORR activity), the N-content steadily increased from 3.0 to 3.5 at % after 24–100 h of immersion (negative shift of 200 mV for the ORR half-wave potential measured with RDE). In that study, the H_2O_2 treatment corresponds to 1.5–10^{-2} mol H_2O_2 mg^{-1} and was also performed at 80°C.[26,69] The N-speciation after ex situ H_2O_2 treatment was not discussed, but after fuel cell testing for 500 h a relative increase in pyrrolic N was also observed on the N_{1s} spectrum.[26]

Changes in the N content and speciation of the Cr-N-C catalysts are now discussed. For Cr-N-C, a fifth N component was necessary for fitting the N_{1s} spectrum. Its BE of 396.5–396.7 eV corresponds to CrN.[70] The small N content assigned to CrN is explained on the basis of the smaller penetration depth of X-rays in CrN (Table II). Thus, the N_{1s} spectrum of Cr-N-C is practically unmodified by the presence of CrN and largely reflects N-moieties integrated in the carbon matrix. While pristine Cr-N-C shows contents of pyrrolic, graphitic and oxidized N similar to those of pristine Fe-N-C and Co-N-C, its content of pyridinic N is significantly higher, 3.08 vs. 1.75 at % for Fe- and Co-N-C (Table III). Similar to Fe- and Co-N-C, the content of pyrrolic N in Cr-N-C increased after H_2O_2 treatment (+0.85 at %). In contrast to Fe- and Co-N-C, the content of pyridinic N decreased strongly (−1.06 at %). Since CrN particles are not known to be active toward ORR, the activity of Cr-N-C is assigned to highly basic N-groups formed in the carbon matrix during NH_3 pyrolysis.[16,58] The strong decrease of pyridinic N in Cr-N-C with H_2O_2 treatment might explain the strong decrease in ORR activity of that catalyst after H_2O_2 treatment (Fig. 4c).

The oxygen content and speciation is now discussed (Table II). The total O-content increased dramatically after H_2O_2 treatment for Fe-N-C (+8.2 at %), Co-N-C (+4.3 at %) and Cr-N-C (+6.3 at %). The larger increase of O-content in Fe-N-C vs. Co-N-C is positively correlated with a larger decrease in ORR activity (Figs. 5 & 7). The O_{1s} spectra were fitted with four components, labelled O1 to O4 (Table II). The O1 component is assigned to oxygen doubly bonded with C as in C=O or O=C-OH, O2 is assigned to C-O-H or C-O-C groups and O3 to oxygen singly-bonded with C as in O=C-OH or O=C-OR.[71] The increase of the O1 and O2 components in Fe-N-C, Co-N-C and Cr-N-C accounts for the major part of the total increase in O-content after H_2O_2 treatment. The largest increase is observed for C-O-H (hydroxyl) and C-O-C (epoxide). Those groups are known to result in strong distortion of the graphene layers due to sp^3 hybridization of carbon atoms.[72] In graphene oxide, this distortion leads to a interlayer spacing of 6.7 Å, ca twice that in graphite.[73] The increase in total O-content on Fe-N-C after treatment with 10^{-2} mol H_2O_2 mg^{-1} (+8.4 at %) is very similar to the value of +8.0 at % oxygen reported for a PANI-Fe-C catalyst over a 500 h PEMFC test at 0.4 V.[26] Surface oxidation of carbon thus seems to be the main degradation route during reaction with H_2O_2. The inclusion of large amounts of oxygen on the edge of graphene sheets or on the basal planes may have dramatically changed the electronic properties of the surface, as reported for graphene nano-ribbons.[74–75] The Co-N-C catalyst was however less oxidized than Fe-N-C and Cr-N-C after treatment with 10^{-2} mol H_2O_2 mg^{-1}. This agrees with the trends in fluoride measurement and collection yield previously discussed (Fig. 9). For Co-N-C, the weight gain of 6% observed after treatment with 10^{-2} mol H_2O_2 mg^{-1} is commensurate with the increase in O-content measured by XPS (+4.3 at. %). Hence, it seems that no carbon atoms initially present in Co-N-C were lost during the treatment with 10^{-2} mol H_2O_2 mg^{-1}, and oxygen atoms grafted on the catalyst surface.

Comparison between ex situ H_2O_2 degradation and operando *fuel cell degradation.*— In this section, we focus on the Fe-N-C catalyst. The polarization curves of a PEMFC with a loading of 4 mg cm^{-2} of pristine Fe-N-C at the cathode have been recorded at BoL and after different duration of galvanostatic operation at 0.5 A cm^{-2} (Fig. 15, solid lines). A galvanostatic control was chosen in order to easily calculate the electric charge that passed through the cathode. The polarization curves measured at BoL of cathodes comprising Fe-N-C catalysts after treatment with H_2O_2 are also shown (dashed and dashed-dot curves). As can be seen, the BoL curve for Fe-N-C treated with 10^{-2} mol H_2O_2 per mg corresponds to ca 76–100 h of operation

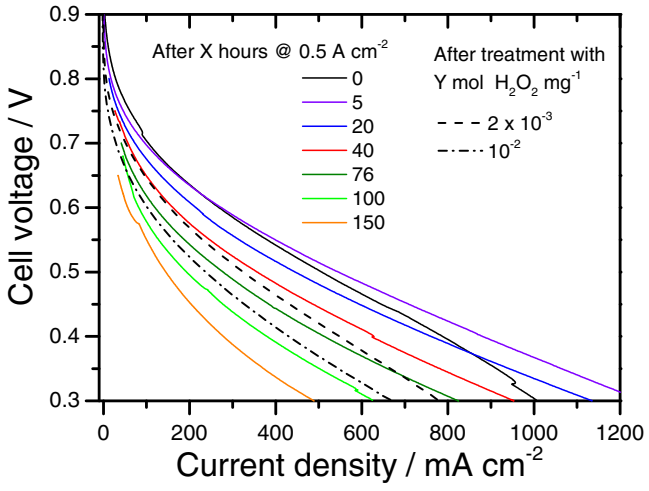

Figure 15. PEMFC polarization curves for cathodes comprising the pristine Fe-N-C and measured after X hours of operation in fuel cell at 0.5 A cm^{-2} (solid lines) and for cathodes comprising Fe-N-C catalysts treated with Y mol H_2O_2 per mg and measured at BoL (dashed or dash-dot lines).

Author Proof

in fuel cell at 0.5 A cm^{-2}. If H_2O_2 released during ORR in fuel cell is the most important cause of degradation under steady state operation, the cumulative amount of H_2O_2 produced after 76–100 h at 0.5 A cm^{-2} and normalized by the mass of catalyst in the cathode should be similar to the amount of 10^{-2} mol H_2O_2 per mg used for the ex situ degradation. The calculation of that scalar for *operando* conditions now only requires a hypothesis on the % H_2O_2 produced during ORR on the Fe-N-C catalyst. This % H_2O_2 can be assumed on the basis of the RRDE measurements on pristine Fe-N-C (Fig. 6).

To calculate the cumulative number of mol H_2O_2 produced in fuel cell after X hours, we now derive its expression as a function of the steady-state current density of the fuel cell, the duration of operation and the % H_2O_2 during ORR. When the PEMFC operates at 0.5 A cm^{-2} with a cathode catalyst loading of 4 mg cm^{-2}, then the electric current produced by every mg of catalyst is 0.5/4 = 0.125 A. After e.g. 100 h of operation, the electric charge passed per mg of catalyst is $100 \times 3600 \times 0.125 = 4.5 \times 10^4$ C mg^{-1}, equivalent to 0.466 mol of electrons per mg of catalyst. If the % H_2O_2 produced as a by-product of the ORR is 5% (5 mol H_2O_2 produced for 100 mol of reacted O_2), then it ensues that 5 mol H_2O_2 are produced for 390 mol of electrons. The latter scalar comes from 5 mol H_2O_2 x2 electrons/H_2O_2 + 95 mol H_2O x4 electrons/H_2O. The scalar of 0.466 mol electrons per mg can now be converted to the scalar mol H_2O_2 per mg catalyst by multiplying it by 5/390. This yields 5.97×10^{-3} mol H_2O_2 per mg. It represents the number of mol H_2O_2 that 1 mg of Fe-N-C catalyst has produced over 100 h of operation at 0.5 A cm^{-2}. Based on the above reasoning, the general equation relating the % H_2O_2 (x) during ORR with the ratio mole H_2O_2 per mol of electrons is:

$$\text{mol}\,H_2O_2/\text{mol electrons} = R1 = x/(400 - 2x) \quad [1]$$

Also, the general relation between the current density, I, duration of PEMFC operation at that current density, Δt, and the ratio of mol electrons per mg catalyst is:

$$\text{mol electrons/mg catalyst} = R2 = I\,\Delta t/\,(FL) \quad [2]$$

Where I is the current density in A cm^{-2}, Δt is the duration in seconds, F Faraday's constant in S.I. units and L the cathode catalyst loading in mg cm^{-2}. From equations 1 and 2, the ratio of mol H_2O_2 per mg catalyst can be expressed as:

$$\text{mol}\,H_2O_2\,\text{per mg catalyst} = R1 \cdot R2 = x\,I\,\Delta t/[FL(400 - 2x)] \quad [3]$$

Applying this equation with x = 5, I = 0.5 A cm^{-2}, Δt = 76 h or 100 h and L = 4 mg cm^{-2}, the scalars of $4.5 \cdot 10^{-3}$ and $6 \cdot 10^{-3}$ mol H_2O_2 per mg catalyst are calculated. The fair agreement between polarisation curves measured after 100 h of operation and that for the Fe-N-C catalyst treated with 10^{-2} mol H_2O_2 per mg catalyst suggests that the formation of 5% H_2O_2 as a by-product of ORR is a possible explanation for the degradation of the Fe-N-C catalyst under relatively high load (0.5 A cm^{-2}). The hypothesis of 5% H_2O_2 during ORR in PEMFC is not contradicting the RRDE measurements performed on pristine Fe-N-C (Fig. 6). The % H_2O_2 measured at low loading in RRDE varied between 2.5 and 3.3% in the range of 0.2–0.5 V vs. RHE. In conclusion, for Fe-N-C, the scalar mol H_2O_2 per mg catalyst predicts both the ex situ and the *operando* degradation. The underlying cause of the degradation is however believed to be the formation of ROS from the decomposition of H_2O_2 on FeN_xC_y moieties.

Conclusions

Ex situ degradation with H_2O_2 of a Fe-N-C, a Co-N-C and a Cr-N-C catalyst was investigated. The negative effect on the ORR activity and fuel cell performance was worse for Cr-N-C, followed by Fe-N-C and least for Co-N-C. The initial activity of Cr-N-C is assigned to surface N-groups while the initial activity of Fe-N-C and Co-N-C is assigned to MeN_xC_y moieties integrated in the carbon matrix. These moieties accounted for ca 80 and 90% of the metal atoms in the pristine Co- and Fe-N-C catalysts, respectively. The changes observed with X-ray absorption and Mössbauer spectroscopy before and after degradation with H_2O_2 were minor. Most of the MeN_xC_y moieties present in the pristine catalysts were still present in the Fe- and Co-N-C catalysts after degradation with 10^{-2} mol H_2O_2 mg^{-1}. The relative loss of Fe and Co content was 17 and 27%. In parallel, the ORR activity at 0.8 V vs. RHE was divided by ca 6–10 for Fe-N-C and 3 for Co-N-C. The super-proportional decrease of ORR activity with decreased metal content can be interpreted in two ways: either only a fraction of the MeN_xC_y moieties are on the top surface in pristine catalysts, or the turnover frequency for ORR of the MeN_xC_y moieties remaining after degradation with H_2O_2 was drastically decreased. A technique able to distinguish between MeN_xC_y moieties situated in the bulk and those located on the surface is needed to draw final a conclusion. The H_2O_2 chemical treatment oxidized the surface of the catalysts, resulting in +4 to +8 atom % oxygen. The oxidizing species is believed to be radical oxygen species (ROS) generated via a Fenton reaction between transition metal centres and H_2O_2. This is supported by the lower fluoride concentration and lower degradation measured for Co-N-C than for Fe-N-C after peroxide treatment. From a comparison between ex situ and *operando* degradation, the chemical attack of Fe-N-C by H_2O_2 seems to be the main degradation mechanism in steady-state operation. To mitigate this main degradation mechanism, four approaches can be envisaged for Me-N-C catalysts: i) synthesis of catalysts with minimized % H_2O_2 during oxygen reduction, ii) synthesis of catalysts or cathodes with a more graphitic structure, iii) synthesis of catalysts that do not form ROS in the presence of H_2O_2, iv) addition of radical scavengers.

Acknowledgments

We acknowledge funding from ANR, contract 2011 CHEX 004 01 and Synchrotron SOLEIL (Gif-sur Yvette, France) for provision of synchrotron radiation facilities at beamline SAMBA (proposal 20131078). Moulay Sougrati (UMR 5253, Montpellier) is acknowledged for analysis of the Mössbauer spectra.

References

1. M. Debe, *Nature*, **486**, 43 (2012).
2. F. Jaouen, E. Proietti, M. Lefèvre, R. Chenitz, J. P. Dodelet, G. Wu, H. T. Chung, C. M. Johnston, and P. Zelenay, *Energy Environ. Sci.*, **4**, 114 (2011).
3. F. T. Wagner, B. Lakshmanan, and M. F. Mathias, *J. Phys. Chem. Lett.*, **1**, 2204 (2010).
4. A. Rabis, P. Rodriguez, and T. J. Schmidt, *ACS Catal.*, **2**, 864 (2012).
5. H. A. Gasteiger, S. S. Kocha, B. Sompalli, and F. T. Wagner, *Appl. Catal. B-Environ.*, **56**, 9 (2005).
6. B. D. James, J. A. Kalinoski, and K. N. Baum, http://www1.eere.energy.gov/hydrogenandfuelcells/pdfs/dti_80kwW_fc_system_cost_analysis_report_2010.pdf, accessed 11-11-2012.
7. R. Jasinski, *Nature*, **201**, 1212 (1964).
8. M. Lefèvre, E. Proietti, F. Jaouen, and J. P. Dodelet, *Science*, **324**, 71 (2009).
9. E. Proietti, F. Jaouen, M. Lefèvre, N. Larouche, J. Tian, J. Herranz, and J. P. Dodelet, *Nature Commun.*, **2**, 416 (2011).
10. G. Wu, K. L. More, C. M. Johnston, and P. Zelenay, *Science*, **332**, 443 (2011).
11. D. Zhao, J.-L. Shui, L. R. Grabstanowicz, C. Chen, S. M. Commet, T. Xu, J. Lu, and D. J. Liu, *Adv. Mater.*, **26**, 1093 (2014).
12. S.-T. Chang, C.-H. Wang, H.-Y. Du, H.-C. Hsu, C.-M. Kang, C.-C. Chen, C.-S. Wu, S.-C. Yen, W.-F. Huang, L.-C. Chen, M.-C. Lin, and K.-H. Chen, *Energy Environ. Sci.*, **5**, 5305 (2012).
13. J. Tian, A. Morozan, M. T. Sougrati, M. Lefèvre, R. Chenitz, J. P. Dodelet, D. Jones, and F. Jaouen, *Angew. Chem. Int. Ed.*, **52**, 6867 (2013).
14. A. Serov, K. Artyushkova, and P. Atanassov, *Adv. Energy Mater.*, **4**, 1301735 (2014).
15. N. Larouche, R. Chenitz, M. Lefèvre, E. Proietti, and J. P. Dodelet, *Electrochim. Acta*, **115**, 170 (2014).
16. J. Herranz, F. Jaouen, M. Lefèvre, U. I. Kramm, E. Proietti, J. P. Dodelet, P. Bogdanoff, S. Fiechter, I. Abs-wurmbach, P. Bertrand, T. M. Arruda, and S. Mukerjee, *J. Phys. Chem. C*, **115**, 16087 (2011).
17. M. Ferrandon, J. A. Kropf, D. J. Myers, K. Artyushkova, U. I. Kramm, P. Bogdanoff, G. Wu, C. M. Johnston, and P. Zelenay, *J. Phys. Chem. C*, **116**, 16001 (2012).
18. T. Han, N. Dale, K. Adjemian, V. Nallathambi, and S. C. Barton, *Electrochem. Soc. Trans.*, **41**, 2289 (2011). Q2
19. G. Liu, X. Li, P. Ganesan, and B. N. Popov, *Appl. Catal. B-Environ.*, **93**, 156 (2009).
20. G. Liu, X. Li, and B. N. Popov, *Electrochem. Soc. Trans.*, **25**, 1251 (2009).
21. V. Goellner, C. Baldizzone, A. Schuppert, M. T. Sougrati, K. J. J. Mayrhofer, and F. Jaouen, *Phys. Chem. Chem. Phys.*, **16**, 18454 (2014).
22. U. I. Kramm, M. Lefèvre, P. Bogdanoff, D. Schmeisser, and J. P. Dodelet, *J. Phys. Chem. Lett.*, **5**, 3750 (2014).
23. F. Charreteur, F. Jaouen, and J. P. Dodelet, *Electrochim. Acta*, **54**, 6622 (2009).

Author Proof

24. S. Baranton, C. Coutanceau, C. Roux, F. Hahn, and J. M. Léger, *J. Electroanal. Chem.*, **577**, 223 (2005).
25. M. Lefèvre and J. P. Dodelet, *Electrochim. Acta*, **48**, 2749 (2003).
26. G. Wu, K. Artyushkova, M. Ferrandon, J. Kropf, D. Myers, and P. Zelenay, *Electrochem. Soc. Trans.*, **25**, 1299 (2009).
27. A. Muthukrishnan, Y. Nabae, T. Hayakawa, T. Okajima, and T. Ohsaka, *Catal. Sci. Technol.*, **5**, 475 (2015).
28. M. Ferrandon, X. Wang, J. Kropf, D. Myers, G. Wu, C. M. Johnston, and P. Zelenay, *Electrochim. Acta*, **110**, 282 (2013).
29. U. I. Kramm, I. Herrmann-Geppert, S. Fiechter, G. Zehl, I. Zizak, I. Dorbandt, D. Schmeisser, and P. Bogdanoff, *J. Mater. Chem. A*, **2**, 2663 (2014).
30. Z. Siroma, N. Fujiwara, T. Ioroi, S.-I. Yamazaki, H. Senoh, K. Yasuda, and K. Tanimoto, *J. Power Sources*, **172**, 155 (2007).
31. J. P. Meyers and R. M. Darling, *J. Electrochem. Soc.*, **153**, A1432 (2006).
32. C. A. Reiser, L. Bregoli, T. W. Patterson, J. S. Yi, D. Yang, M. L. Perry, and T. D. Jarvi, *Electrochem. Solid State Lett.*, **8**, A273 (2005).
33. F. Jaouen and J. P. Dodelet, *J. Phys. Chem. C*, **113**, 15422 (2009).
34. N. Ramaswamy and S. Mukerjee, *Adv. Phys. Chem.*, **2012**, 491604 (2012).
35. J. Chlistunoff, *J. Phys. Chem. C*, **115**, 6496 (2011).
36. J. D. Wiggins-Camacho and K. J. Stevenson, *J. Phys. Chem. C*, **115**, 20002 (2011).
37. I. Katsounaros, W. B. Schneider, J. C. Meier, U. Benedikt, U. P. Biedermann, A. A. Auer, and K. J. J. Mayrhofer, *Phys. Chem. Chem. Phys.*, **14**, 7384 (2012).
38. F. Haber and J. Weiss, *Proceedings of the Royal Society of London. Series A, Mathematical and Physical Sciences*, **147**, 332 (1934).
39. I. M. Kolthoff and A. I. Medalia, *J. Am. Chem. Soc.*, **71**, 3777 (1949).
40. W. G. Barb, J. H. Baxendale, P. George, and K. R. Hargrave, *Faraday discussions*, **47**, 462 (1951).
41. K. Wiesener, *Electrochim. Acta*, **31**, 1073 (1986).
42. F. H. Lu and H. Y. Chen, *Thin solid films*, 398, 368 (2001).
43. M. Sevilla and A. B. Fuertes, *Carbon*, **44**, 468 (2006).
44. F. J. Maldonado-Hódar, C. Moreno-Castilla, J. Rivera-Utrilla, Y. Hanzawa, and Y. Yamada, *Langmuir*, **16**, 4367 (2000).
45. A. Zitolo, V. Goellner, F. Emiliano, M. T. Sougrati, L. Stievano, and F. Jaouen, submitted (2015).
46. J. M. Ziegelbauer, T. S. Olson, S. Pylypenko, F. Alamgir, C. Jaye, P. Atanassov, and S. Mukerjee, *J. Phys. Chem. C*, **112**, 8839 (2008).
47. F. Jaouen, in *Non-noble metal fuel cell catalysts*, Wiley -VCH, Weinheim (2014) 29.
48. N. Ramaswamy, U. Tylus, Q. Jia, and S. Mukerjee, *J. Am. Chem. Soc.*, **135**, 15443 (2013).
49. A. Bonakdarpour, M. Lefèvre, R. Yang, F. Jaouen, T. Dahn, J. P. Dodelet, and J. R. Dahn, *Electrochem. Solid-State Lett.*, **11**, B105 (2008).
50. E. F. Holby, G. Wu, P. Zelenay, and C. D. Taylor, *J. Phys. Chem. C*, **118**, 14388 (2014).
51. C. E. Szakacs, M. Lefèvre, U. I. Kramm, J. P. Dodelet, and F. Vidal, *Phys. Chem. Chem. Phys.*, **16**, 13654 (2014).
52. E. F. Holby and C. D. Taylor, *Appl. Phys. Lett.*, **101**, 064102 (2012).
53. S. Kattel and G. Wang, *J. Materials Chem. A*, **1**, 10790 (2013).
54. S. Kattel, P. Atanassov, and B. Kiefer, *Phys. Chem. Chem. Phys.*, **15**, 148 (2013).
55. J. Sun, Y.-H. Fang, and Z.-P. Liu, *Phys. Chem. Chem. Phys.*, **16**, 13733 (2014).
56. F. Jaouen, M. Lefèvre, J. P. Dodelet, and M. Cai, *J. Phys. Chem. B*, **110**, 5553 (2006).
57. F. Charreteur, F. Jaouen, S. Ruggeri, and J. P. Dodelet, *Electrochim. Acta*, **53**, 2925 (2008).
58. U. I. Kramm, J. Herranz, N. Larouche, T. M. Arruda, M. Lefèvre, F. Jaouen, P. Bogdanoff, S. Fiechter, I. Abs-Wurmbach, S. Mukerjee, and J. P. Dodelet, *Phys. Chem. Chem. Phys.*, **14**, 11673 (2012).
59. U. I. Koslowski, I. Abs-wurmbach, S. Fiechter, and P. Bogdanoff, *J. Phys. Chem. C*, **112**, 15356 (2008).
60. A. Morozan, M. T. Sougrati, V. Goellner, D. Jones, L. Stievano, and F. Jaouen, *Electrochim. Acta*, **119**, 192 (2014).
61. U. I. Kramm, I. abs-Wurmbach, I. Herrmann-Geppert, J. Radnik, S. Fiechter, and P. Bogdanoff, *J. Electrochem. Soc.*, **158**, B69 (2011).
62. C. A. Melendres, *J. Phys. Chem.*, **84**, 1936 (1980).
63. T. Ruskov, S. Asenov, I. Spirov, C. Garcia, I. Mönch, A. Graff, R. Kozhuharova, A. Leonhardt, T. Mühl, M. Ritschel, C. M. Schneider, and S. Groudeva-Zotova, *J. Appl. Phys.*, **96**, 7514 (2004).
64. F. Jaouen, J. Herranz, M. Lefèvre, J. P. Dodelet, U. I. Kramm, P. Herrmann, P. Bogdanoff, J. Maruyama, T. Nagaoka, A. Garsuch, J. R. Dahn, T. Olson, S. Pylypenko, P. Atanassov, and E. Ustinov, *Appl. Mater. Interf.*, **1**, 1623 (2009).
65. H. Schulenburg, S. Stankov, V. Schünemann, J. Radnik, I. Dorbandt, S. Fiechter, P. Bogdanoff, and H. Tributsch, *J. Phys. Chem. B*, **107**, 9034 (2003).
66. K. Artyushkova, S. Levendosky, P. Atanassov, and J. Fulghum, *Top. Catal.*, **46**, 263 (2007).
67. K. Artyushkova, S. Pylypenko, T. Olson, J. E. Fulghum, and P. Atanassov, *Langmuir*, **24**, 9082 (2008).
68. J. Casanovas, J. M. Ricart, J. Rubio, F. Illas, and J. M. Jimenz-Mateos, *J. Am. Chem. Soc.*, **118**, 8071 (1996).
69. Personal communication with Dr Piotr Zelenay, October 2014. The H_2O_2 degradation protocol in that study involved 100 mg catalyst immersed in 500 ml of 10 wt% H_2O_2.
70. A. Conde, A. B. Cristobal, G. Fuentes, T. Tate, and J. de Damborenea, *Surface & coatings technology*, **201**, 3588 (2006).
71. R. Rozada, J. I. Paredes, S. Villar-Rodil, A. Martinez-Alonso, and J. M. D. Tascon, *Nano Res.*, **6**, 216 (2013).
72. J.-A. Yan, L. Xian, and M. Y. Chou, *Phys. Rev. Lett.*, **103**, 086802 (2009).
73. D. Pandey, R. Reifenberger, and R. Piner, *Surf. Sci.*, **602**, 1607 (2008).
74. E. J. Kan, Z. Q. Li, J. Yang, and J. G. Hou, *J. Am. Chem. Soc.*, **130**, 4224 (2008).
75. Q. Tang, Z. Zhou, and Z. Chen, *Nanoscale*, **5**, 4541 (2013).

Author Proof

Queries

Q1: Table III is not set in this paper, so please check call out Table III for correctness.
Q2: AU: Please provide a digital object identifier (doi) for Ref(s) 18, 20, 26, 34, and 42. For additional information on doi's please select this link: http://www.doi.org/. If a doi is not available, no other information is needed from you.